Journal of Zhejiang University SCIENCE A
ISSN 1009-3095
http://www.zju.edu.cn/jzus
E-mail: jzus@zju.edu.cn

Beam steering in planar photonic crystal based on its anomalous dispersive properties

WU Li-jun[†1,2], MAZILU M.[1], GALLET J.F.[1], KRAUSS T.F.[1]

([1]*The Ultrafast Photonics Collaboration, School of Physics & Astronomy, University of St. Andrews, St. Andrews, Fife KY16 9SS, Scotland, UK*)

([2]*Department of Physics, Hong Kong University of Science and Technology, Hong Kong, China*)

[†]E-mail: phljwu@ust.hk

Received Sept. 5, 2005; revision accepted Oct. 10, 2005

Abstract: We utilize the anomalous dispersion of planar photonic crystals near the dielectric band edge to control the wavelength-dependent propagation of light. We typically observe an angular swing of up to 10° as the input wavelength is changed from 1290 nm to 1310 nm, which signifies an angular dispersion of 0.5°/nm ("Superprism" phenomenon). Such a strong angular dispersion is of the order required for WDM systems. By tuning the incident angle, light beams with up to 20° divergence were collimated over a 25 nm (1285 nm to 1310 nm) bandwidth using a triangular lattice ("Supercollimator" phenomenon). The wavelength collimating range can be extended from 25 nm to 40 nm by changing the lattice from triangular to square. These two devices can be realized in the same configuration, simply by tuning the wavelength. Sources of loss are discussed.

Key words: Planar photonic crystals, Superprism, Supercollimator, Anomalous dispersive properties
doi:10.1631/jzus.2006.A0045 **Document code:** A **CLC number:** O441; TN204

INTRODUCTION

Photonic crystals (PhCs) are increasingly attracting attention due to their ability of controlling light propagation on a wavelength scale, by which a fascinating platform for a new generation of integrated optical devices and components can be provided. Many studies on PhCs however, focused on new means of tailoring the emission and propagation of light using the photonic band gap (PBG) property whereby the photon density of states is zero. A PhC with a full PBG resembles an insulator where the Fermi energy lies in the energy gap. Besides being used as insulators, PhCs can also be employed as photonic conductors because of their interesting dispersive properties, especially near the bandgap (Notomi, 2000). Recently, by varying the wavelength and incident angle, respectively, Kosaka *et al*.(1998; 1999a; 1999b; 2000) demonstrated "Superprism" and "Supercollimator" phenomena as well as spot-size conversion in their "autocloned" 3-dimensional (3D) photonic crystals. The autocloned structure has very favourable properties, but requires specialized non-standard fabrication techniques. Planar photonic crystals, in contrast, are much more suited for novel integrated optics applications because of their relative ease of fabrication compared to 3D systems (Krauss *et al*., 1996). They use two-dimensional (2D) lattices to confine and manipulate the light in plane, and total internal reflection of a multilayer slab structure to confine light vertically. The disadvantage of using a 2D PhC is that light near the Γ point is poorly confined (large out-of plane wavevector component) and we need to use a different operating point other than that successfully employed in the autocloned system. Therefore, we choose to design our PhC conductive devices near the symmetry point (K or M in the hexagonal case and X or M in the square case), because the vertical confinement offered by our waveguide is relatively weak, so $\boldsymbol{k}$ has to have its main component in the plane of the crystal.

In the following, we will first introduce the

simulation method, the fabrication procedure and measurement setup. Then superprism, self-collimating phenomena in the planar PhCs will be discussed. The devices demonstrated here are GaAs/AlGaAs-based semiconductor structures, which provide the required high refractive index contrast (Δn>2) and have a mature fabrication technology. All experimental work is conducted in the "holes in dielectric" instead of the reverse "pillars in air" geometry because of its connected nature and the fact that the dielectric provides the required vertical confinement.

SIMULATION

We use plane-wave expansion (PWE) method to calculate the photonic band structure (PBS) and Equi-frequency dispersion contours (EFDCs). The direction of propagation light in the PhCs is normal to the EFDC, since the energy velocity is identical with the group velocity, which is given by $v_g=\nabla_\kappa\omega(\kappa)$. Together with the momentum conservation rule, the propagation direction can be worked out from the incident wave-vector in the EFDC.

In the calculation, the effective index of the waveguide slab is used as the refractive index of the semiconductor host, verified by identifying the photonic band edge in separate transmission measurements. The fill-factor of the lattice is approximated from SEM micrographs.

As a more intuitive way to display the light propagation direction in the PhCs, we also apply FDTD method to model the device designed by PWE calculation. A 2D model is sufficient for the purpose as the photonic functionality only depends on the 2D lattice. Perfectly matched layer boundaries were chosen to allow the radiation to leave the boundary without reflecting back inside. The grid size for modelling is set to $a/20$, where a is the lattice spacing.

FABRICATION AND MEASUREMENT

The devices designed by PWE and FDTD modelling results were then patterned into a 200 nm thick layer of electron beam resist (Polymethylmethacylate, PMMA) by E-beam lithography. Following the development of the resist, the pattern is transferred to the SiO_2 mask layer via fluorine-based etch chemistry (CHF_3). Using chemically assisted ion beam etching (CAIBE), the pattern is transferred into the semiconductor. The whole procedure is summarized in Fig.1. The ratio between the hole radius and lattice constant (r/a) is designed as 1/3, which was shown to be successful in previous experiments (Krauss *et al.*, 1996).

The schematic diagram for the measurement setup is shown in Fig.2. The semiconductor laser (Agilent 8167B) has a tuneable wavelength range extending from 1255 nm to 1365 nm. The light is injected via a normal cleaved single-mode fibre (SMF) or a cylindrically lensed fibre. As shown in Fig.3, there is a significant incompatibility between the normal SMF and the input waveguide, which will result

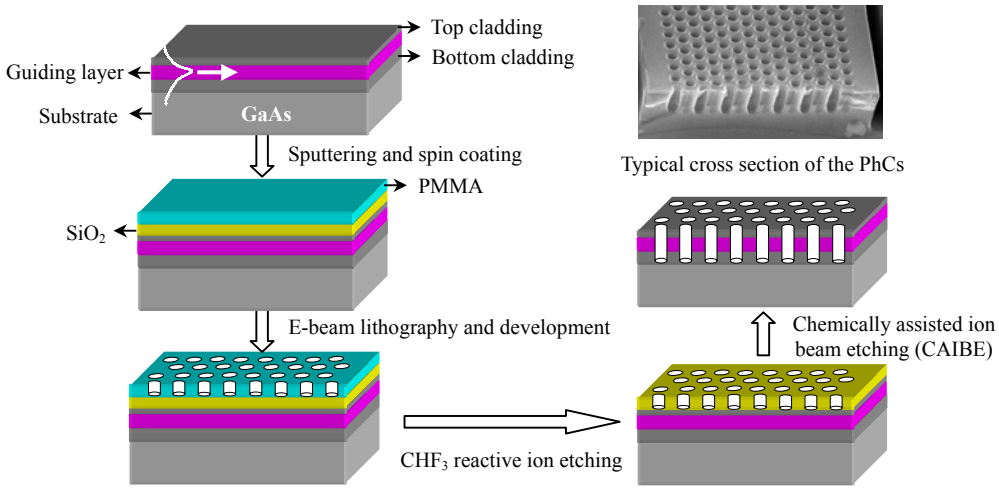

Fig.1 Sample fabrication procedure

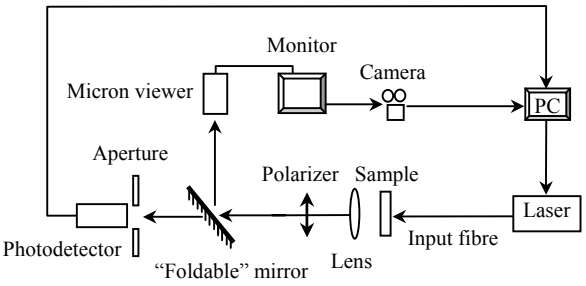

Fig.2 Schematic diagram of the measuring setup

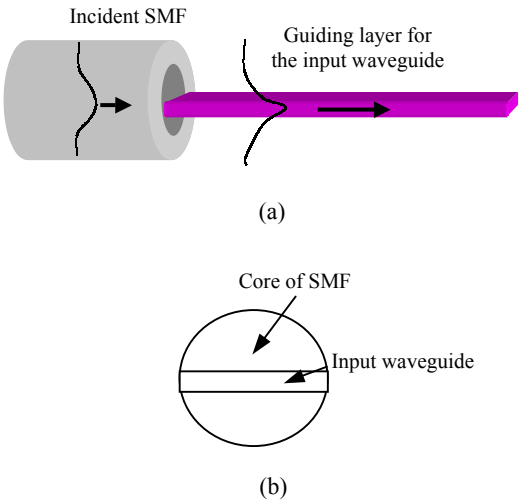

Fig.3 Illustration of the incompatibility between the normal SMF and the input waveguide of the device. Normally, the thickness of the guiding layer of the waveuguide is from 250 nm to 400 nm. Applying a normal SMF with 7 μm as core diameter, there is a significant vertical incompatibility, resulting in high insertion loss. Therefore, a cylindrically lensed fibre to squeeze the mode into the propagating plane is necessary to couple more light into the input waveguide. (a) Side view; (b) End view

in high insertion loss. Therefore, a cylindrically lensed fibre to squeeze the mode into the propagating plane is highly required to couple more light into the input waveguide.

One vidicon camera is used to observe the output facet of the sample and another one is used with a 50× long working distance objective to obtain top view images of the sample. The output facet is imaged by an aspheric lens and the polarisation is selected via a Wollaston prism. An iris aperture is used to spatially filter out any scattered light and guarantee that only the waveguided light is incident upon a Ge PN large area detector (New Focus 2033). Finally, a lock-in amplifier detects the transmitted signal as the laser is scanned across its tuning range with constant output power. Video images of the output facet of the sample are shown at different input wavelengths, which have been mounted together in order to show the evolution with wavelength.

SUPERPRISM PHENOMENON (Wu *et al*., 2002)

Figs.4a and 4b show the scanning electron microscope (SEM) pictures of the top views for the superprism with input and output waveguides and the interface between the input waveguide and photonic crystals. The input waveguide, which was chosen 10 μm wide to avoid strong diffraction at its output and to generate a quasi-parallel input for the superprism, is tilted at 25° from normal to the crystal edge (the incident edge is Γ-M). The shape for the crystal area was designed as a semicircle to ensure the light to be transported out straightforward from the crystals (to first approximation). The 10 μm output waveguides designed to pick up the output light are orientated at divisions of 10° from −70° to 70°, which leads to the large space between the crystal area and the output waveguide.

Figs.4c and 4d exhibit the video images of the output facet of the sample at different input wavelengths. The light swings from the 30º to the 40º waveguide as the input wavelength is changed from 1290 nm to 1310 nm (Fig.4c). The multiple spots in each waveguide here are due to higher order modes excited in the 10 μm wide output waveguides. Note that when the wavelength is between 1295 nm and 1305 nm, there are spots in both the 30° and 40° waveguides. We attribute this to that the swing of the light in this range is less than 10° and the direction of propagation is somewhere between the 30° and the 40° waveguides, so the signal couples into both waveguides.

The physical mechanism behind this effect can be explained with the EFDC of the PBS. Fig.5 shows the PBS (TE-like mode) and EFDCs at frequencies of 0.214 and 0.217 (in units of c/a. Same in the following context). Note that near the band gap, the propagation direction will be changed acutely even if there is just a very small variation of the incident angle (Fig.5b).

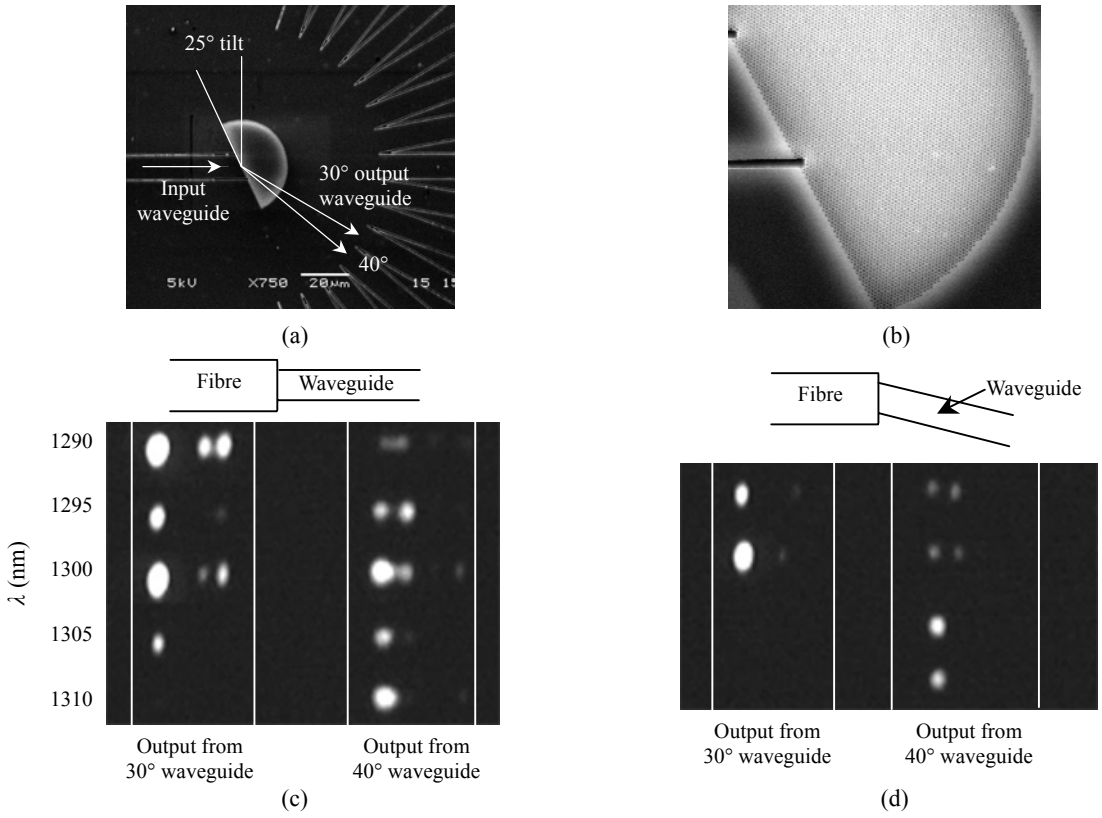

Fig.4 (a) SEM top view of photonic crystals with input and output waveguides; (b) Close image of the PhC area; (c), (d) Vidicon photographs for the output light spots at different wavelengths. It is shown that when the input waveguide matches well with the fibre (c), the light swings from the 30° to the 40° waveguide as the input wavelength is changed from 1290 nm to 1310 nm. Rotating the sample by about 8° with respect to the cleaved facet, the same swing is observed for a smaller change in wavelength, i.e., from 1300 nm to 1305 nm

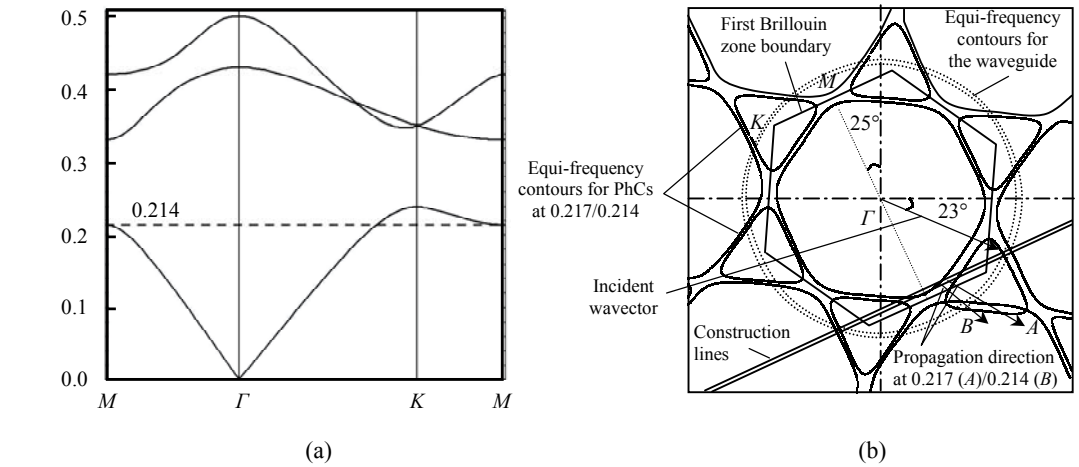

Fig.5 (a) PBS (TE-like mode) for the PhCs used for the superprism demonstrated here. The dashed horizontal line corresponds to one of the frequency we used in the experiment; (b) EFDSs for the first band. The solid lines are those for the PhCs and the dashed lines represent the uniform semiconductor waveguides. The EFDSs were rotated by 25° to match with the experiment situation, where the incident edge *Γ*-*M* is tilted at 25° from the vertical direction. From this picture, it can be seen that when the wavelength is altered by 20 nm (the frequency changes from 0.217 c/a to 0.214 c/a), the propagation direction swings by 10° (from *A* to *B*) assuming the input mode is incident at −23° to the direction of the waveguide

Furthermore, given a very small change of the input wavelength (frequency in the wavevector diagram), the shape of the equi-frequency curves experiences a large alteration. In Fig.5b, when the frequency is altered from 0.214 c/a to 0.217 c/a, which corresponds to a wavelength change from 1310 nm to 1290 nm when a=280 nm, the shape of the equi-frequency contour varies from a quasi-hexagram to a quasi-triangle.

However, to explain this experimental result by the EFDC is not so straightforward here even if we account for a reasonable experimental error in all parameters involved. We then remeasured the waveguides and found that the results depended, in part, on the alignment between the input fibre and the 10 μm semiconductor waveguide that feeds into the superprism. This is emphasized in Fig.4b, which shows a higher angular dispersion when the input fibre is tilted slightly. This gave us the critical clue: The input waveguide has a few imperfections on it, which may favour a few specific higher order modes. Higher order modes can be understood to propagate along a zig-zag path and therefore do not enter the crystal at the normal angle. By scanning through the different possible angles, we then found that a propagation angle of the waveguided light of 23° to normal yields the observed swing from 30° to 40° in the superprism described above. Considering the size (10 μm) and refractive index contrast (>3:1) of the waveguide, a zig-zag path of 23° does not appear unreasonable and is well within the range allowed by total internal reflection. By adjusting the model, and assuming that the incident light was at 20° to waveguide normal, we were able to explain our observation after all. In Fig.5b, assuming the input mode is incident at 23°, it impinges on the superprism as shown and yields output angles of 30° and 40° for the frequencies corresponding to the wavelengths 1290 nm and 1310 nm.

The 10° light swing for the change of wavelength from 1290 nm to 1310 nm demonstrated here corresponds to a 0.3° light swing when the wavelength is changed from 1550 nm to 1550.8 nm (ITU grid for 100 GHz separation). To project the possible performance of the superprism in a WDM system, we extrapolated our result as shown in Fig.6: For a separation of the output waveguides of 3 μm, the device would have to be 500 μm long. Assuming the beam was collimated, it could be coupled into PhC waveguides separated by 3 μm and such waveguides would have a typical crosstalk of approximately 30 dB. Therefore, the angular dispersion of 0.5°/nm observed in our superprism is of the order required for WDM systems. Furthermore, being realized in a 2D structure, this superprism is easily combined with other planar optical components such as ridge waveguides, 60° bends and *Y* couplers, which makes it attractive for applications in the ultracompact photonic integrated circuits.

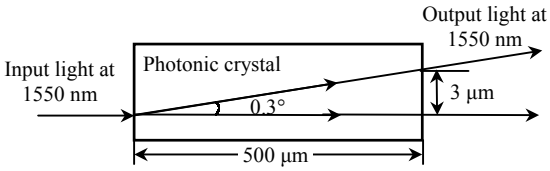

Fig.6 Schematic for the application of the superprism demonstrated in this paper

SELF-COLLIMATING PHENOMENON (Wu *et al*., 2003a; 2003b)

As illustrated above, PhC lattices are very promising candidates for ultracompact wavelength-selective components. To realize this functionality, it is necessary to precisely control the spatial profile of the light propagation through the PhC lattice. Propagation without divergence is particularly desirable in such systems.

To obtain non-divergent light propagation in PhCs, it is necessary to find a flat section in EFDC to collimate the divergent incident beam. Fig.7a illustrates the EFDCs for the hexagonal lattice at frequencies 0.236, 0.248 and 0.254 c/a. As can be seen, the shape of the EFDC changes from convex to concave when the frequency varies from 0.236 c/a to 0.254 c/a. This implies that between these two frequencies, there should be a region with flat EFDC section. We then choose operating frequency at 0.248 c/a. As shown in Fig.7b, in the incident angle range of ±10°, the light in the PhCs propagates along Γ-K direction, representing that light in the entire ±10° range will be collimated by the crystal. Furthermore, as the frequency is changed from 0.236 c/a to 0.248 c/a and then to 0.254 c/a, the propagation angle in the PhCs swings from 0° to −10° and then to −20° (Fig.7a). These swings represent that the superprism

phenomenon can be realized together with the supercollimator effect. FDTD modelling results are exhibited in Figs.7c~7f, showing the field distributions for the *H*-mode at different wavelengths (a=320 nm). As the results from PWE simulation, the light swings from −20° to −10° and then to 0° when the frequency changes from 0.254 c/a (λ=1260 nm) to 0.248 c/a (λ=1290 nm) and 0.237 c/a (λ=1350 nm).

Fabricated hexagonal supercollimator is shown in Fig.8. We explored the relationship between the width of the input waveguide and its diffraction effect. The conclusion is that 5 μm is enough to obtain quasi-parallel input if the input fibre and sample are aligned properly. Compared to the superprism we demonstrate above (Fig.4), this width will obviously improve the situation for multimodedness. The 3 μm output waveguides were designed to extend into the PhCs to avoid the effect of the output interface. During

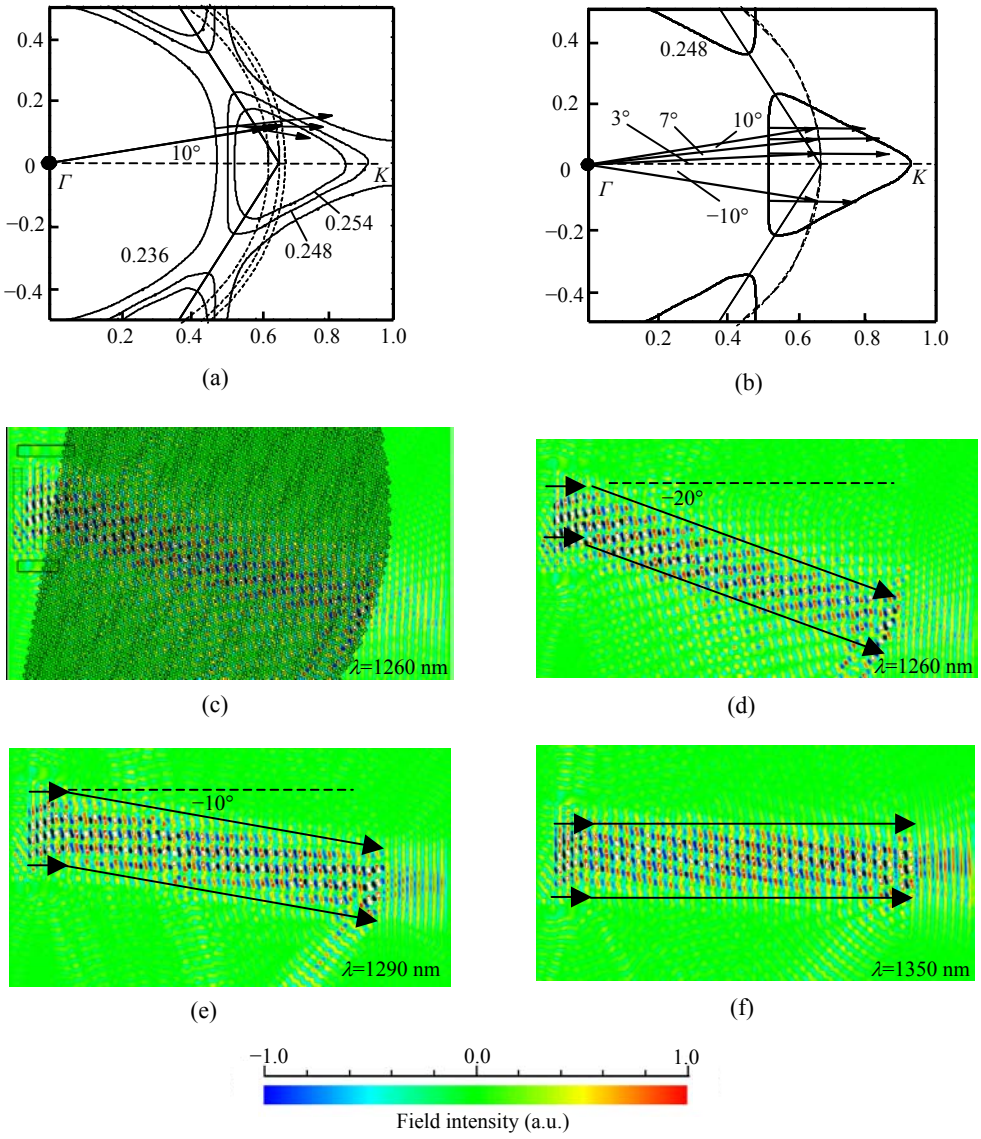

Fig.7 (a) EFDSs at frequencies 0.236 c/a, 0.248 c/a and 0.254 c/a for the different incident angles of 3°, 7°, 10°, −10°; (b) EFDS at frequency 0.248 c/a. This graph clearly indicates that in the incident angle range of ±10°, the light in the PhCs will propagate along *Γ*-*K* direction, representing the case of collimation; (c)~(e) Field distribution for *H*-mode at different wavelengths. Cases (c) and (d) are identical, except that the air-holes are shown in (b) for illustration (a=320 nm). A Gaussian beam with width of 5 μm is launched 2 μm away from the input interface. From these FDTD simulation results, it can be seen that light swings from −20° (d) to −10° (e) and then to 0° (f) when the wavelength changes from 1260 nm to 1290 nm and 1350 nm. These results are consistent with PWE simulation

the fabrication, we mapped the lattice constants from 250 nm to 350 nm considering the experimental error. For example, the fill-factor for PhCs will be dependent on the exposure dose from the E-beam lithography.

Fig.9 illustrates the measurement results. In Fig.9a, it can be seen that when the wavelength is in the range of 1285~1310 nm (corresponding to 0.249~0.244 c/a at a=320 nm), the transmission from −10° output waveguide is dominant, meaning that the light propagates through the crystal along Γ-K direction. To give a more intuitive picture, we show the top view of the crystals in Fig.9b. The dashed lines represent the outline of the PhC area and the input waveguide. Again, at 1310 nm, the light exits the PhCs at −10°, i.e., along Γ-K direction, so the photonic crystal acts as a collimator as shown in the simulation.

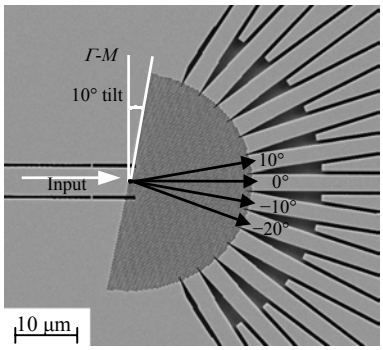

(a)

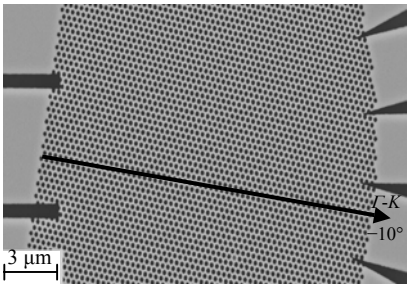

(b)

Fig.8 (a) SEM for the hexagonal supercollimator with the input waveguide being tilted 10° from normal to the crystal edge (the incident edge is Γ-M); (b) Enlarged central section of (a), highlighting the input and output interfaces between the access waveguides and photonic crystals

Fig.9c displays the transmission spectra for the spots at 10°, 0°, −10°, −20° output waveguides, respectively, with the scattered points representing the raw data. The strong oscillation of the transmission that

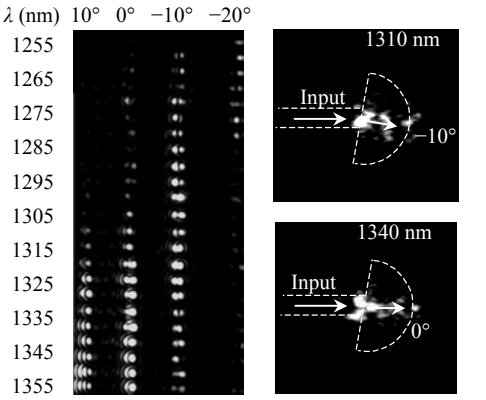

(a) (b)

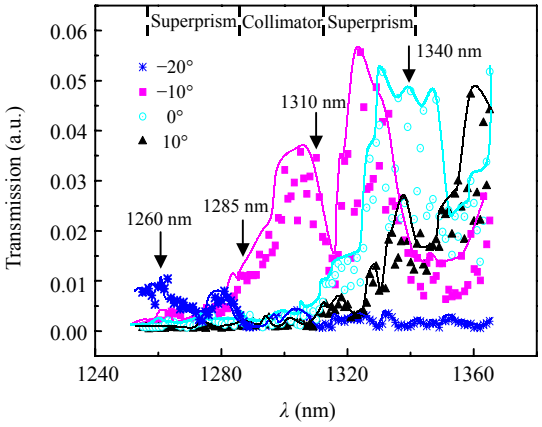

(c)

Fig.9 (a) Measured vidicon micrographs. It is shown that when the wavelength is in the range of 1285~1310 nm, the transmission from −10° output waveguide is dominant, which means the light is propagating in the PhCs along the Γ-K direction and collimated. With the increase of the wavelength (from 1310 nm to 1340 nm), the light swings from the −10° waveguide to the 0° and 10° waveguides; (b) Top view of the PhCs at the wavelength of 1340 nm and 1310 nm. It can be seen that at 1310 nm, the light exits the PhCs at −10°, i.e., along Γ-K direction, so the PhC acts as a collimator. At 1340 nm, the light mainly propagates through the PhCs at 0°, i.e., straight through. These two top views agree well with the output facet results as shown in (a); (c) The transmission spectra for the spots at 10°, 0°, −10°, −20° output waveguides, respectively. Besides the collimation from 1285 nm to 1310 nm and the superprism effect from 1310 nm to 1340 nm, there is a third regime between 1260 nm and 1285 nm, where the light swings from −20° to −10°, which can be understood as a second superprism regime

appears like noise is due to Fabry-Perot resonances between the cleaved input facet and the first crystal interface, as discussed further below. As the Fabry-Perot resonances cause destructive interference in transmission, the peak amplitudes of the oscillations represent the true transmission. Therefore, we have connected the peak transmission points in the raw data together as a visual aid. These spectra allow us to make the same observation as the side views of Fig.9a, i.e., that from 1285 nm to 1310 nm, the light is collimated along the *Γ-K* direction of the crystal and therefore couples into the −10° output waveguide. These experimental results are consistent with the PWE and FDTD modelling. It is worth noting that in the collimator case, there is very clean transmission in one direction only, as highlighted by the high observed contrast to other output waveguides of about 9:1, which means that scattering into other directions and excitation of other modes in the PhC is small.

In Fig.9a, with the increase of the wavelength (from 1310 nm to 1340 nm), the light swings from the −10° waveguide to the 0° and 10° waveguides. Diffraction patterns (the lobes in the 1325~1365 nm wavelength range at the adjacent 10° and 0° output waveguides) are visible here outside of the transmission spots because of the small size (3 μm) of the output waveguides.

The quantitative transmission spectra in Fig.9c display the same swing as in Fig.9a, from −10° to 0° and 10°. A similar swing from the −20° to −10° waveguide, which is not so obvious in the qualitative measurement, can also be observed when the wavelength is changed from 1260 nm to 1285 nm, although the transmission is weak. The light propagating along −20° is negatively refracted by 10° from normal to the input interface.

However, the collimating bandwidth of the hexagonal lattice is not very large (only 25 nm). Recently, Witzens *et al*.(2002) showed numerically that the square lattice has favorable properties for collimation applications, but no experimental results were shown in their paper. We designed a square lattice collimator based on PWE and FDTD simulation (Wu *et al*., 2003a). The experiment results are illustrated in Fig.10. Fig.10a demonstrates the SEM of the square supercollimator. In Fig.10b and Fig.10c, it is clearly shown that the collimating bandwidth is extended to 40 nm (1260~1300 nm).

DISCUSSION

Losses

Loss analyses were conducted on the hexagonal supercollimator. In order to obtain a quantitative estimate of the losses, we have compared the transmission through an unperturbed 5 μm wide waveguide of the same length as the waveguide-PhC system described here, and measured approximately 2% transmission for the waveguide-PhC system. From the

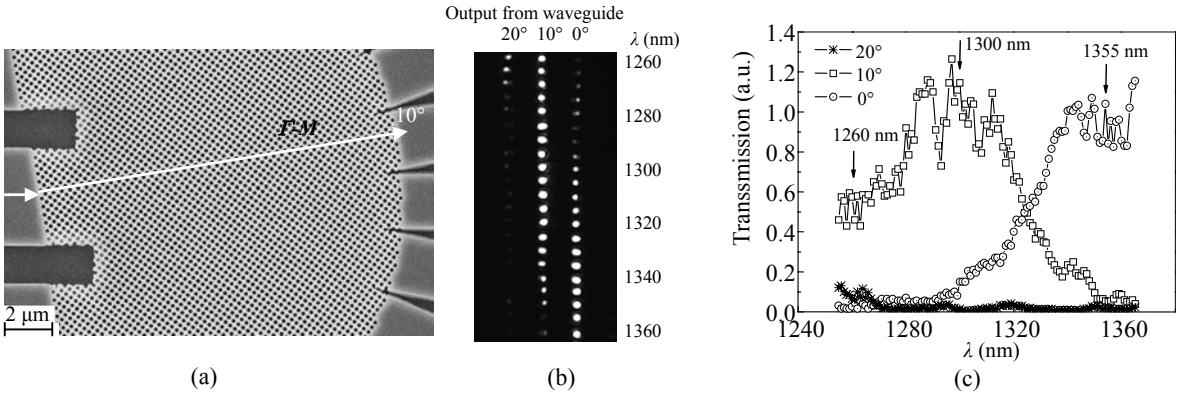

Fig.10 (a) SEM for the fabricated square supercollimator. The design for input and output waveguides is similar to that for the hexagonal supercollimator; (b) Vidicon micrographs for the output light spots at different wavelengths. When the wavelength is in the range of 1260~1300 nm, the transmission from 10° output waveguide is dominant, which means the light is propagating in the PhCs along the *Γ-M* direction and collimated. With the increase of the wavelength (from 1300 nm to 1355 nm), the light swings from the 10° waveguide to the 0° waveguide; (c) The transmission spectra for the spots at 20°, 10°, 0° output waveguides, respectively. This quantitive measurement also displays the collimating regime (1260~1300 nm) and the light swinging (from 10° to 0°) regime (from 1300 nm to 1355 nm) as in (b)

top view of the PhCs area in Fig.9b, it is straightforward to recognize that the interface between the input waveguide and PhC is a major source of this loss. This observation is confirmed by high resolution scans of the transmission from the 0° waveguide (Fig.11), which shows clear oscillations with $\Delta\lambda$~0.6 nm wavelength spacing, corresponding to 0.55 mm cavity size. This size accurately reflects the length between the cleaved input facet and the first waveguide-PhC interface, so this interface is a major source of reflective loss. A possible way to reduce the reflection is to change the discrete interface between the waveguide and the PhC to a more graded interface, similar to the type proposed by Baba and Ohsaki (2001) and Baba and Nakamura (2002) where much improved transmission was calculated via FDTD simulations.

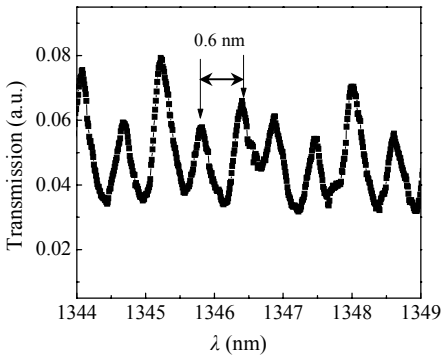

Fig.11 High resolution scans of the transmission from the 0° waveguide in Fig.9, which shows clear oscillations with $\Delta\lambda$~0.6 nm wavelength spacing, corresponding to 0.55 mm cavity size. This size accurately reflects the length between the cleaved input facet and the input waveguide-PhC interface

Another source of loss is the intrinsic propagation loss of the weakly confined vertical waveguide used here. The only reason we can observe light propagation in these crystals is the out-of-plane scattering, which is obviously undesirable and needs to be improved, either by deeper etching or improved waveguide design.

Real device design

As can be seen from the transmission spectra in Fig.9, the line-widths of the transmission peaks are broad (~40 nm). This can cause cross-talk between neighbor channels and reduce the resolution of the superprism. Possible solutions include adding another part to focus the output from the PhC area or filtering the output signal (Witzens *et al*., 2005; Jugessur *et al*., 2005). Also the ***k***-distribution of the incident light will degrade the resolution of the superprism. This problem could be improved by adding a supercollimtor at the beginning of the superprism part to parallelize the input for the superprism as shown in Fig.12.

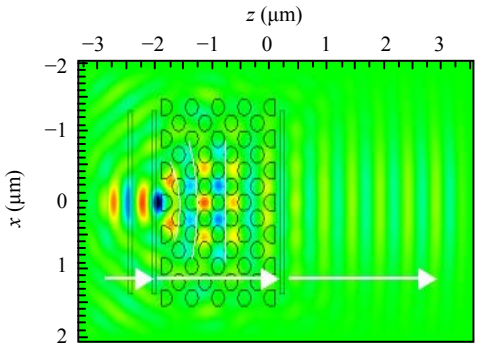

Fig.12 The incident Gaussian beam can be collimated by a very compact PhC collimator

In Fig.5b, the 2°/nm resolution of the superprism cannot be explained if we only consider the effect of the input interface between the PhC-waveguide. Have a look at the output interface between the PhC-waveguide, it can be seen that the output interface of the PhC area is not along symmetrical direction such as Γ-M or Γ-K, which will lead to another modification for the light propagation direction similar to the effect of the input interface. If we design the output interface properly, the superprism effect could be enhanced by the output interface.

CONCLUSION

We utilize the anomalous dispersion of planar photonic crystals near the dielectric band edge to control the wavelength-dependent propagation of light. We typically observe an angular swing of up to 10° as the input wavelength is changed from 1290 nm to 1310 nm, which signifies an angular dispersion of 0.5°/nm ("Superprism" phenomenon). Such a strong angular dispersion is of the order required for WDM

systems. By tuning the incident angle, light beams with up to 20° divergence were collimated over a 25 nm (1285 nm to 1310 nm) bandwidth using a triangular lattice ("Supercollimator" phenomenon). The wavelength collimating range can be extended from 25 nm to 40 nm by changing the lattice from triangular to square. These two devices can be realized in the same configuration, simply by tuning the wavelength. Sources of loss and several points related to the design of the devices are discussed.

References

Baba, T., Ohsaki, D., 2001. Interfaces of photonic crystals for high efficiency light transmission. *Jpn. J. Appl. Phys*., **40**:5920-5924, Part 1. [doi:10.1143/JJAP.40.5920]

Baba, T., Nakamura, M., 2002. Photonic crystal light deflection devices using the superprism effect. *IEEE J. Quan. Electron.*, **38**:908-914.

Jugessur, A.S., Bakhtazad, A., Wu, L., Kirk, A., Krauss, T.F., de la Rue, R.M., 2005. A compact and integrated 2-D photonic crystal superprism filter-device for wavelength demultiplexing applications. Submitted.

Kosaka, H., Kawashima, T., Tomita, A., Notomi, M., Tamamura, T., Sato, T., Kawakami, S., 1998. Superprism phenomena in photonic crystals. *Phys. Rev. B*, **58**: R10096-R10099. [doi:10.1103/PhysRevB.58.R10096]

Kosaka, H., Kawashima, T., Tomita, A., Notomi, M., Tamamura, T., Sato, T., Kawakami, S., 1999a. Superprism phenomena in photonic crystals: Toward microscale lightwave circuits. *J. Lightwar Technol.*, **17**:2032-2038. [doi:10.1109/50.802991]

Kosaka, H., Kawashima, T., Tomita, A., Notomi, M., Tamamura, T., Sato, T., Kawakami, S., 1999b. Self-collimating phenomena in photonic crystals. *Appl. Phys. Lett.*, **74**:1212-1214. [doi:10.1063/1.123502]

Kosaka, H., Kawashima, T., Tomita, A., Sato, T., Kawakami, S., 2000. Photonic-crystal spot-size converter. *Appl. Phys. Lett.*, **76**:268-270. [doi:10.1063/1.125743]

Krauss, T.F., de la Rue, R.M., Brand, S., 1996. Two-dimensional photonic-bandgap structures operating at near-infrared wavelengths. *Nature*, **383**:699-702. [doi:10.1038/383699a0]

Notomi, M., 2000. Theory of light propagation in strongly modulated photonic crystals: Refractionlike behaviour in the vicinity of the photonic band gap. *Phys. Rev. B*, **62**:10696-10705. [doi:10.1103/PhysRevB.62.10696]

Witzens, J., Loncar, M., Acherer, A., 2002. Self-collimation in planar photonic crystals. *IEEE J. Selected Topics in Quantum Electron*., **8**:1246-1257. [doi:10.1109/JSTQE.2002.806693]

Witzens, J., Baehr-Jones, T., Scherer, A., 2005. Hybrid superprism with low insertion losses and suppressed cross-talk. *Phys. Rev. E*, **71**:026604. [doi:10.1103/PhysRevE.71.026604]

Wu, L., Mazilu, M., Karle, T., Krauss, T.F., 2002. Superprism phenomena in planar photonic crystals. *IEEE J. Quan. Electron.*, **38**:915-918. [doi:10.1109/JQE.2002.1017607]

Wu, L., Mazilu, M., Krauss, T.F., 2003a. Beam steering in planar-photonic crystals: From superprism to supercollimator. *J. Lightwave Tech.*, **21**:561-566. [doi:10.1109/JLT.2003.808773]

Wu, L., Mazilu, M., Gallet, J.F., Krauss, T.F., 2003b. Square lattice photonic-crystal collimator. *Photonics and Nanostructures–Fundamentals and Applications*, **1**:31-36. [doi:10.1016/S1569-4410(03)00004-X]